Large Eddy Simulation of Flow-Field and Micro-Particle Deposition in an Idealized Mouth-Throat

X.G. Cui*, E. Gutheil
Interdisziplinäres Zentrum für Wissenschaftliches Rechnen, Ruprecht-Karls-Universität Heidelberg, Im Neuenheimer Feld 368, 69120 Heidelberg, Germany

Abstract

The study concerns the simulation of the flow field and particle deposition in the upper human respiratory system. The numerical simulations are conducted using large eddy simulation (LES) and a Lagrangian particle tracking technique. To validate the numerical methods, the average gas velocity at the centerline and at different cross-sections in a constricted tube is compared with the experimental data [1] and numerical data from Reynolds-averaged Navier–Stokes (RANS) equations coupled with low Reynolds number (LRN) κ-ω model [2] and LRN shear-stress transport (SST) κ-ω model [3] from literature. Through the comparison, it is concluded that the present methodology is suitable to simulate the laminar–transitional–turbulent flow. In addition, the particle deposition efficiency in the idealized mouth-throat model is compared with data from the literature [2]. It demonstrates that the methodology can be used to predict particle deposition in the human oral airway. The main properties of the flow field in the idealized geometry are captured as other numerical simulation [2], but a small recirculation zone was observed in the posterior side of pharynx and laryngeal jet is observed to impinge on the anterior side of trachea wall in the present numerical result. The secondary vortices are attributed to the laryngeal jet profile.

Introduction

Aerosol particle deposition of therapeutic agents remains an essential tool in current treatment methods for asthma and other lung diseases. The advantage of pulmonary drug delivery through inhalation is that it offers topical treatment of specific lung conditions while limiting the whole-body effects [4]. The extra-thoracic region, including the nasal and oral passages, pharynx, and larynx, build the entrance to the human respiratory tract [5]. The therapeutic aerosol particles, drugs can be directly transported via the oral airway to the lung. Aerosol particles deposition in this region has important implications in drug delivery efficiency [5]. So, it is very important to study the airflow structures and particle transport for filtering effects in the oral airway [2].

One challenge for numerical simulation in this region is its geometric complexity [2]. There are a lot of previous numerical simulations that have been done on the idealized mouth-throat models [3]. According to dimensions of a human cast reported by Cheng et al. [6], an idealized oral airway model including mouth cavity, pharynx, larynx and trachea was built by Kleinstreuer *et al*. [7]. A series of research work [2,7-10] was done on this geometry model. For instance, the flow field and micro-particle transport in the idealized mouth-throat were simulated by Zhang *et al*. [2]. The numerical results in the simplified model exhibit the main features of laminar-transitional-turbulent particle suspension flow in the human oral airways. Moreover, it shows that the turbulence may enhance the particle deposition in the trachea near the larynx, in particular, for the particle deposition of smaller particles. In 2004, the airflow and transport of nano-particles were analyzed by Zhang and Kleinstreuer [8] for both unsteady and steady inspiration flow rates in a upper airway including the oral airway. It is observed that the transient effects of flow field in oral airway mainly appear during the decelerating phase of inspiration circle. Another idealized mouth-throat was built by Stapleton *et al*. [11]. It was constructed on the information from literature, computed tomography (CT) scans, magnetic resonance imaging (MRI) scans, and direct observation of living subjects. Many numerical simulations [11-16] concern the mouth-throat model. Recently, numerical simulations using the realistic geometry are performed. The deposition pattern in a CT-based realistic airway configuration was analyzed by Jayarajua *et al*. [3]. The numerical results of flow show that the laminar to turbulent transition, especially at low flow rates, is sensitive to the complexity of the airway model. In fact, flow transition is seen soon after the glottis region for a low flow rate of 15 L/min, but which are not reported in the simplified geometry simulations [3].

Another challenge is that the flow ranges from laminar, transitional and turbulent within the respiratory system, which requires the method not only to capture laminar flows, but also transitional and turbulent flow structures [17]. Most of previous work used the RANS method to simulate the flow field. In 2001, Stapleton et al. [11] adopted the κ-ε model to simulate the flow field using a Lagrangian tracking method coupled with the eddy interaction model to simulate the fluid-particle in a simplified mouth-throat model. It is observed that the model

*Corresponding author: Xinguang.Cui@iwr.uni-heidelberg.de

failed to predict the flow field in the relatively high flow rate and it is not suitable for the accurate prediction of particle deposition [11]. Four different turbulent models such as LRN κ-ε model, renormalization group (RNG) κ-ε model [18], which uses renormalization group method to account for the effects of smaller scales' motion (http://www.cfd-online.com/Wiki/RNG_k-epsilon_model), Menter's κ-ω model [18], which is suitable for high Reynolds number flows and LRN κ-ω, were used by Zhang and Kleinstreuer [18] to simulate the internal flow field in two different test conduits with local constrictions. The LRN κ-ω model is identified to be more suitable to simulate the laminar-transitional-turbulent flow in the constricted tube [18]. The LRN κ-ω model was widely used in numerical simulation of the flow field in the respiratory system [2,7-10]. In addition, LRN SST κ-ω model is proved to predict the transitional flow accurately [3]. The RANS model is suitable for fully developed turbulence, but it may be inappropriate for particle transport in the region with complex flow such as upper respiratory tract [19]. Recently, the prediction of particle deposition has been implemented more and more with large eddy simulation (LES). Luo *et al*. [20] used LES to simulate the flow in a single asymmetric bifurcation model and a constricted tube. It was demonstrated that LES predicts the transitional flow in the constricted tube better than the LRN κ-ε model. Jin *et al*. [14] simulated the flow and micro-particle deposition in a three-dimensional geometric model of human upper respiratory tract. It is found that turbulent dispersion plays an important role in the particle deposition for the particles with small Stokes number. It is observed that particles with the diameter of 1 μm not only deposits on the opposite wall but also on the side wall. Jayarajua *et al*. [19] simulated the fluid flow in a human mouth–throat model under normal breathing condition (30 L/min) alternatively using RANS κ-ω (without near-wall corrections), detached eddy simulation (DES) and LES methods. By comparison with existing experimental data in situations below 5 μm and bigger particles, it is found [19] that for the medication aerosols inhaled at a steady flow rate of 30 L/min, LES and DES provide more accurate results than the RANS κ-ω model in predicting particle deposition.

Also, both the LRN κ-ω and LRN SST κ-ω model have been evaluated for the flow field in the constricted tube through comparison with experimental data and other RANS models, and they are frequently used in the numerical simulation of particles transport and deposition in the respiratory system as mentioned above. However, no comparison has been made for the numerical results using LRN κ-ω, LRN SST κ-ω and LES [17] in the constricted tube. In this paper, the validation of the methodology with LES will be performed through the comparison of flow field in the constricted tube with RANS LRN κ-ω model and RANS LRN SST κ-ω model. Moreover, the flow field and particle deposition in a circular simplified mouth-throat were conducted using LES and a Lagrangian particle tracking method.

Geometrical Models

Two different geometries are used in the numerical simulations. The first one is an axi-symmetric constricted tube with an area reduction of 75 %, which is depicted by a cosine function [18] as:

$$r(z)=\begin{cases} R-\dfrac{R}{2}\cos\left(\dfrac{\pi z}{R}\right) & \text{for} \quad |z|\le D \\ R & \text{for} \quad |z|>D \end{cases} \tag{1}$$

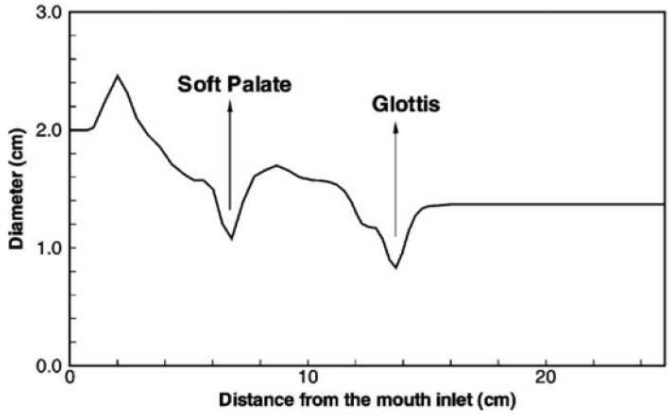

Figure 1. Variations of the cross-sectional diameter with distance from the mouth inlet [7]

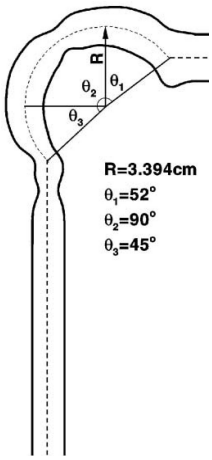

Figure 2. Relation of angle and location of points on the centerline [7]

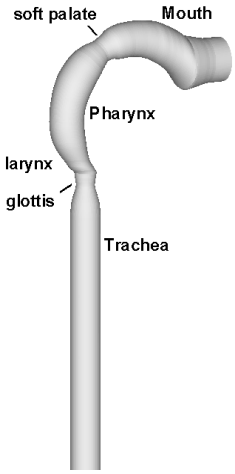

Figure 3. Three-dimensional view of the present idealized mouth-throat geometry

The second configuration consists of a circular cross-section variable mouth-throat, which is developed to get the equivalent "filtering efficiency" with complicated cast models by Kleinstreuer et al. [7]. Diameter variations along the oral airway from the mouth to the trachea coming from the hydraulic diameters of a replicate human oral airway cast [6], which is shown in Fig. 1 [7]. The coordinates of points at the centerline related to different angles are taken from [7], and they are shown in Fig. 2. The variations of the model to the actual cast include the modification in the soft palate, strong bend, smooth tubular wall and a short mouth inlet with a diameter of 2 cm [2]. More details about the idealized mouth-throat model could be referenced to the literature [2, 6, 7]. According to the data mentioned above, a similar mouth-throat with circular cross-section is built, which is shown in Fig. 3.

Methodology

Governing Equations

Neglecting the influence of particles on the fluid, and the interaction between particles, one-way coupling is adopted. For the flow field, three-dimensional (3-D) incompressible Navier-Stokes (N-S) equations are used [14]. LES is applied to treat the turbulence, and the sub-grid scale (SGS) model [21] introduced by Smargorinsky in 1963, is adopted.

If the volume-averaged variance is descried as [14]

$$\bar{\phi}(x,y,z)=\frac{1}{\Delta x\cdot\Delta y\cdot\Delta z}\int_{x-\frac{1}{2}\Delta x}^{x+\frac{1}{2}\Delta x}\int_{y-\frac{1}{2}\Delta y}^{y+\frac{1}{2}\Delta y}\int_{z-\frac{1}{2}\Delta z}^{z+\frac{1}{2}\Delta z}\phi(\xi,\eta,\varphi,t)d\xi d\eta d\varphi \tag{2}$$

then, after the filter processing of physical variables, volume-averaged three-dimension N-S equations [14] can be given as

$$\frac{\partial(\rho\bar{u}_j)}{\partial x_j}=0 \tag{3}$$

$$\frac{\partial\bar{u}_i}{\partial t}=-\frac{\partial}{\partial x_j}\left[\bar{u}_i\bar{u}_j\right]-\frac{\partial}{\partial x_i}\left[\frac{\bar{p}}{\rho}\right]+\frac{\partial}{\partial x_j}\left[\nu\left(\frac{\partial\bar{u}_i}{\partial x_j}+\frac{\partial\bar{u}_j}{\partial x_i}\right)+T_{ij}\right] \tag{4}$$

with the sub-grid scale tensor *Tij*:

$$T_{ij}=\overline{u_iu_j}-\bar{u}_i\bar{u}_j \tag{5}$$

and an eddy-viscosity assumption is adopted to model the SGS tensor [14], then

$$T_{ij} = 2\nu_t \bar{S}_{ij} + \frac{1}{3} T_{ll} \delta_{ij} \tag{6}$$

where

$$\bar{S}_{ij} = \frac{1}{2}\left(\frac{\partial \bar{u}_i}{\partial x_j} + \frac{\partial \bar{u}_j}{\partial x_i} \right) \qquad i, j = 1, 2, 3 \tag{7}$$

$$\nu_t = (C_S \Delta)^2 \left| \bar{S} \right| \tag{8}$$

$$\left| \bar{S} \right| = \left(\bar{S}_{ij} \bar{S}_{ij} \right)^{1/2} \tag{9}$$

$$\Delta = (\Delta x \cdot \Delta y \cdot \Delta z)^{1/3}. \tag{10}$$

The 3-D N–S equations can be rewritten as follows:

$$\frac{\partial (\rho \bar{u}_j)}{\partial x_j} = 0 \tag{11}$$

$$\frac{\partial \bar{u}_i}{\partial t} = -\frac{\partial}{\partial x_j}\left[\bar{u}_i \bar{u}_j \right] - \frac{\partial}{\partial x_i}\left[\frac{\bar{p}}{\rho} \right] + \frac{\partial}{\partial x_j}\left[(\nu + \nu_t)\left(\frac{\partial \bar{u}_i}{\partial x_j} + \frac{\partial \bar{u}_j}{\partial x_i} \right) + T_{ij} \right] \tag{12}$$

Assuming a large particle-to-air density ratio, negligible particle rotation, no inter-particle collision, and drag force as the dominant point force, the Lagrangian equations governing the particle motion [14] are given as follows:

$$m_p \frac{dv_i}{dt} = \frac{\pi d_p^2}{8} C_D \rho \left| u_i - v_i \right| (u_i - v_i) + m_p g_i \tag{13}$$

where the drag coefficient is

$$C_D = \begin{cases} 24 / \mathrm{Re}_p & \text{for} \quad \mathrm{Re}_p \le 0.01 \\ 24 / \mathrm{Re}_p (1 + 0.15 \mathrm{Re}_p^{0.687}) & \text{for} \quad \mathrm{Re}_P > 0.01 \end{cases} \tag{14}$$

The particle Reynolds number is

$$\mathrm{Re}_p = \frac{\rho \left| u_i - v_i \right|}{\mu} \tag{15}$$

Numerical Method

To solve these equations, the open source software platform of OpenFOAM 1.5 (http://www.opencfd.co.uk/Openfoam/) is adopted. A new solver for the flow field with LES and the particle motion with Lagrangian tracking method was constructed based on the solver of oodles and icolagrancianFoam (www.openfoamwiki.net).

The computational grids are generated with Ansys ICEM-CFD 11.0. O-grid is used around the wall surfaces and H-grid is adopted in the center of the geometry. The mesh size is decided until the flow field independent of the number of grid nodes. The final number of grid nodes is 2,771,226 for constricted tube and 1,276,500 grid nodes for the idealized mouth-throat model. The velocity on the inlet surface is 0.473 m/s with 2% fluctuation, corresponding to Re_{in} = 2,000 [1]. The steady inspiration flow rate with 30 L/min corresponding to normal breathing intensity with 2 % fluctuation is implemented. The static relative pressure at the outlet is set to zero. No-slip boundary conditions are adopted on the wall surface.

The particles deposition and transport are studied in the idealized mouth-throat. There are around 10,000 particles injected simultaneously with the air at the inlet plane randomly with the same velocity as the airflow. The particle deposition occurs if the distance of the particle center to the wall is less than half the particle diameter. The particle density is 1,000 kg/m^3. Three diameters d_p = 2, 5, and 10 μm are studied for three different steady inspiration flow rates with 15, 30, and 60 L/min. At this stage, the particle deposition in the flow field is conducted with 103,443 grid nodes.

The computations are carried out in the cluster of bwGrid Cluster at Heidelberg University. A simulation takes around 2 weeks with 56 processors for the flow field in the case of flow inspiration rate of 30 L/min for 1,276,500 grid nodes.

Results and Discussion

Flow Field in the Constricted Tube

The flow field in the constricted tube transits from the laminar to turbulent and the geometry is rather simple with a simple boundary, which qualifies this setting for evaluation of the present method. The results will be compared with the experimental [1] and numerical [2, 3] data. The normalized axial velocity at the centerline and at different cross sections is shown in Fig. 4 and Fig. 5, respectively. In these figures, the velocity is normalized by the mean velocity at the inlet plane, U_{mean}, and the distance in the axial direction is normalized by the tube diameter, D, and in the radial direction with the radius, R, of the tube. From experimental data [1], it is known that the axial flow velocity increases due to area reduction, and it does not change significantly until the location around $Z = 2\ D$. After this relatively steady period, the velocity deceases quickly because of the flow transits from laminar to turbulent coupled with large-scale lateral momentum transfer. In addition, it is described that the flow transition occurs in the region $1 < Z/D < 4$ [1]. The comparison of the velocity at the centerline shown in Fig. 4 shows that the present result fits well with the experimental [1] and numerical [2] results; in particular, in the transitional regime, it performs better than the model of Zhang *et al.* [2].

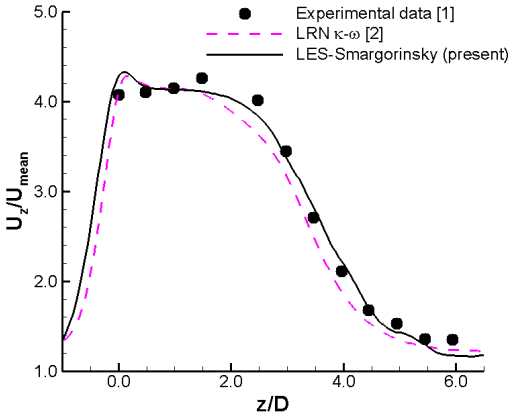

Figure 4. Comparison of the computed centerline velocity with measurements [1] and numerical results [2] for the constricted tube

Detailed comparison of the velocity profile has been performed at different cross-sections. From Fig. 5, it can be observed that the numerical simulations can resolve the evolution of shear layer and recirculation zone.

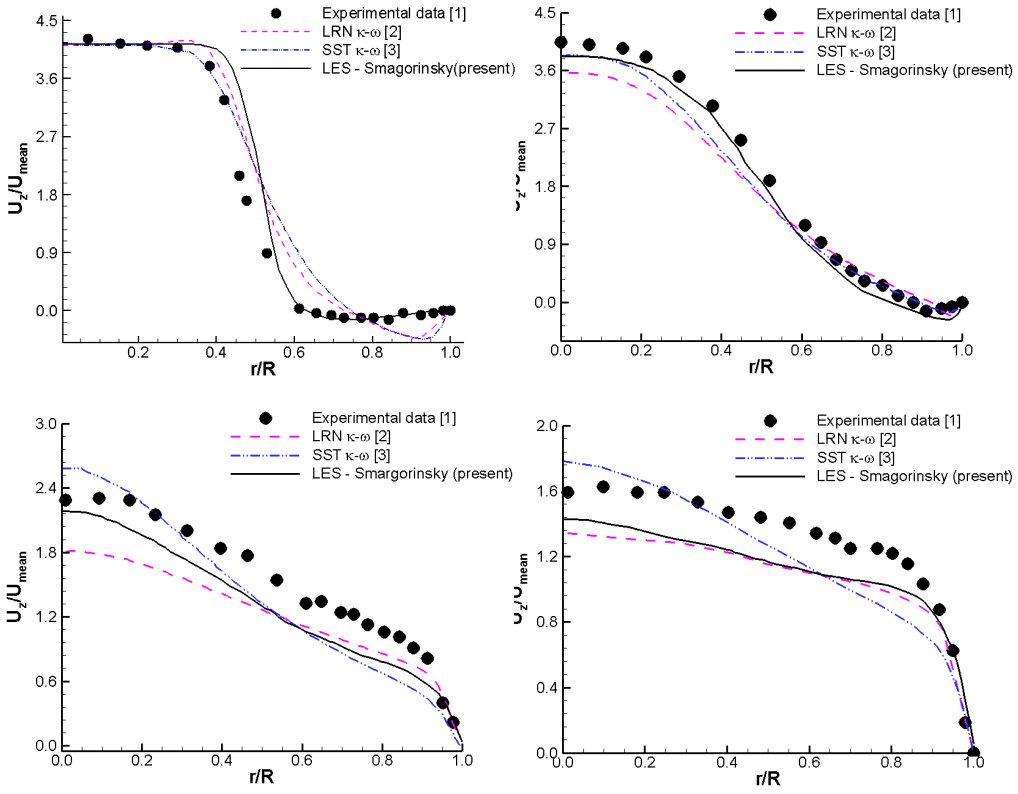

Figure 5. Comparison of normalized axial velocity at different sections downstream of the glottis with experimental data [1] and numerical results [2, 3] at $Z = D$ (top left), $Z = 2.5\ D$ (top right), $Z = 4D$ (bottom right), and $Z = 5D$ (bottom right)

However, the present numerical simulations clearly predict the tendency and the results are much closer to the experimental data [1]. It is observed that the present numerical simulations improve the prediction of the velocity profile in the shear layer region at $Z = D$ in Fig. 5 (top left), and near the center at $Z = 2.5\ D$ (top right). Even though it is not as good as other results in the center region at $Z = D$ and in the peripheral region of the wall at $Z = 2.5\ D$, the general improvement is visible prominently in these regions. At positions $Z = 4\ D$ in Fig. 5 (bottom left) and at $Z = 5\ D$ (bottom right), the general performance of all models is lower than before, the present result is closest to the experimental result and the principal shape is captured. At position $Z = 5\ D$, the velocity profile becomes more blunt and the present result is close to and slightly better than the numerical results of Zhang *et al.* [2] and of Jayaraju *et al.* [3]. It should be emphasized that the discrepancies between experimental and numerical results may also be due to the experimental uncertainty in the region where the velocity varies quickly [20].

In summary, the present numerical method improves the description of the flow field in the constricted tube, in particular in the transition regime. Moreover, the comparison with different models and experiment shows that the present methodology adequately predicts the flow field transition from laminar to turbulent.

In the following section, the second configuration will be studied with the current LES/Smagorinsky formulation.

Flow Field in the Idealized Mouth-Throat

This section addresses the configuration shown in Fig. 3. Figure 6 displays the averaged velocity profile and streamline (left-hand side of Fig. 6) and the axial velocity contour and secondary velocity streamlines at different cross sections (right-hand side of Fig. 6). These cross sections include positions corresponding to the location of oral cavity, pharynx, glottis, as well as one and three diameters of the trachea downstream the glottis in Fig. 6. Positions A - F denote the posterior side, and A' - F' the anterior side.

From the velocity streamline in the mid-plane it can be seen that that the numerical simulation captures the main properties of flow field in the oral airway, including the skewed velocity profile in the oral cavity and pharynx due to centrifugal forces, and flow separation in the lower portion of mouth, in the pharynx region after the soft palate, and downstream of glottis. The asymmetric laryngeal jet extends from the entering location of glottis. There is a small recirculation zone in the posterior side of pharynx and the laryngeal jet is impinging on the anterior wall of trachea, and in contrast to the numerical simulation of Zhang *et al.* [2] in a similar geometry, it is not impinging on the wall. This is probably due to the different geometrical shape nearby the soft palate and glottis. There is a pair of counter vortices in the section of A - A', which is produced because of the pressure gradient. In section B - B', the flow field becomes more complex coupled with the appearance of a recirculation zone. Moreover, there are two big counter-rotating vortices and another pair of smaller vortices residing in this section. In the glottis at section C - C', where the laryngeal jet has appeared, the axial velocity becomes prominent and distributes evenly, which induces weak secondary vortices.

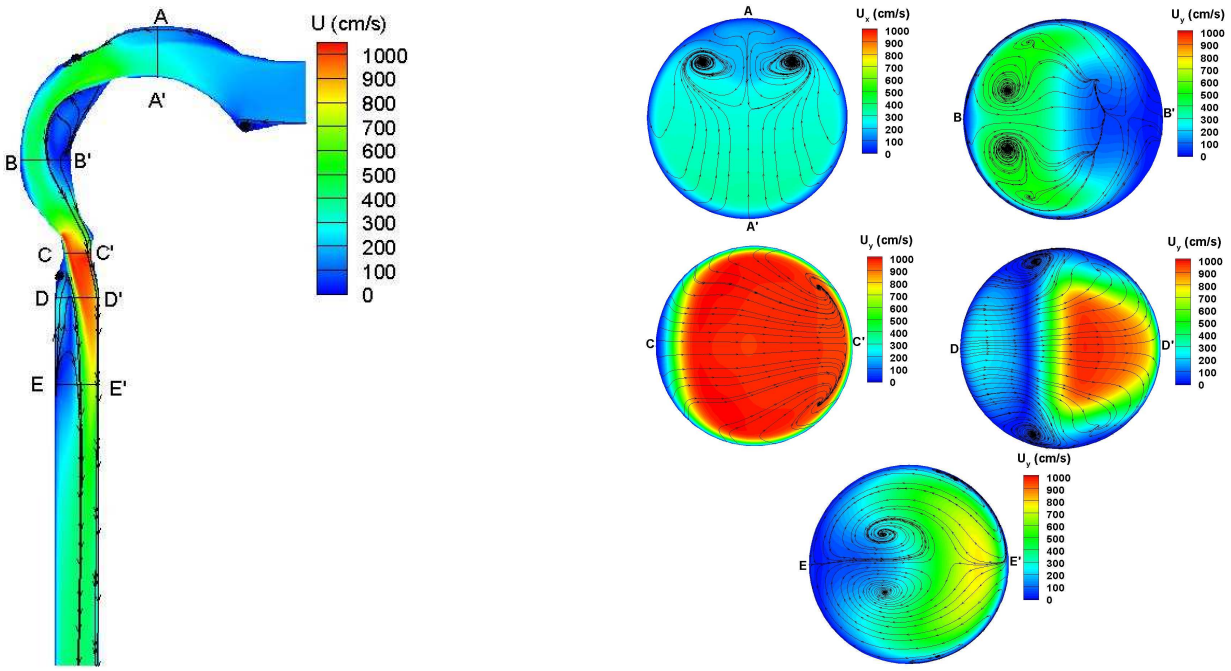

Figure 6. Averaged velocity contour and streamlines at the mid-plane (left), and averaged axial velocity and secondary streamlines at different cross-sections (right)

In addition, at this section, the secondary vortices turn to the anterior side. In section D, where the recirculation zone has appeared and which is at the downstream of laryngeal jet, the highest axial velocity is close to the wall and the vortices appear in the interface of the laryngeal jet and the separation zone. At the section E, which is in the tail of laryngeal jet, the laryngeal jet becomes weak and the axial velocity profile distribution becomes even. The length scale of vortices has increased, and it is located at the interface of recirculation zone and laryngeal jet. From the axial velocity and secondary vortices distribution, it can be summarized that the flow field is very sensitive to the geometrical change in particular in locations with big curvature. The secondary vortices are related with the laryngeal jet and they trend to appear in the boundary of recirculation zone and laryngeal jet.

Particle Deposition

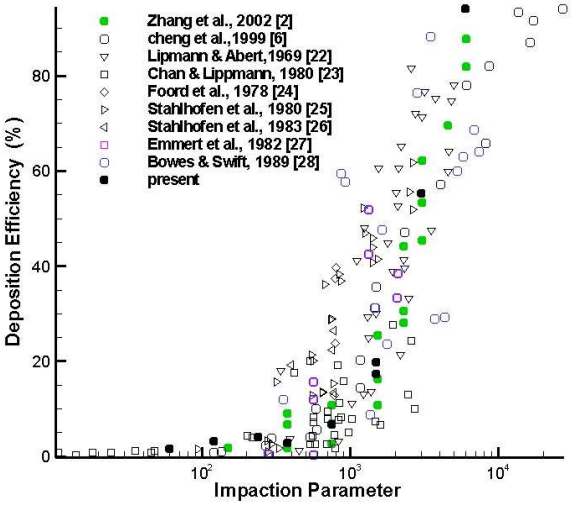

Figure 7. Comparison of numerical particle deposition with experimental [6, 22 -28] and numerical data [2] in the oral airway

A comparison of the present particle deposition efficiency with vivo measurements and other numerical results is a way to evaluate the idealized mouth-throat model [2]. The comparison of the particle deposition efficiency as a function of impaction parameter, $\rho d_p^2 Q$, for the present numerical simulations on the coarse grid with other numerical and experimental results is shown in Fig. 7. For the inertia, impaction is the main mechanism for the micro-size particles' deposition in the oral airway, the particle deposition efficiency increases with increasing impaction parameter. It can be seen that the present results are close to the numerical results from the literature [2]. Moreover, they fit well with the medium trend of the experimental data [2, 6, 22-28], and thus the numerical results are representative values of particle deposition in the human oral airway. Thus, the methodology including the idealized mouth-throat model is suitable to be implemented in the study of particle deposition in the human oral airway.

Conclusions

First, the flow field in a constricted tube was studied with LES and the Smagorinsky model. The velocity at the centerline and velocity profiles at different cross sections downstream the glottis were compared with numerical results and experimental data, in particular with RANS LRN κ-ω model [17]. It is demonstrated that the present methodology can predict the transitional flow in the constricted tube, which sets the base for further studies for the flow field in the simplified mouth-throat model. Moreover, it is found that the velocity profile predicted by the present method is much closer to the experimental data than the other two models, in particular in the transitional regime. In addition, numerical simulations for the flow field in the simplified geometry were presented. The main flow features are observed in the mean flow field in the simplified geometry including a skewed velocity profile, flow separation after the sudden geometric change at the soft plate and glottis and the laryngeal jet. In addition, a small recirculation zone was observed in the posterior side of the pharynx and the laryngeal jet is impinging on the anterior side of trachea, which indicates that the flow field is very sensitive to the geometric profile, in particular, in locations with big curvature. The laryngeal jet profile influences the axial velocity profile, and it changes with the location of laryngeal jet. Both the length scale and location of secondary vortices change with the location of laryngeal jet, and it trends to distribute at the interface of separation zone and laryngeal jet. The particle deposition efficiency corresponding to different particle diameters and steady inspiration flow rates at coarse grid changing with different impaction parameter fit well with numerical results and experimental data. It is concluded that the present methodology is suitable to simulate the particle deposition.

Unsteady flow field is analyzed in a different paper [29]. Future studies focus on the particle motion related with the unsteady flow field. Moreover, numerical studies using generated grids from CT scans will be used to improve the predictability of future studies in this area.

Acknowledgements

The authors gratefully acknowledge financial support of the German Science Foundation (DFG) through International Graduate College 710. They thank the Ministry for Education and Research and the Ministry for Science, Research and Arts Baden-Wuerttemberg for using bwGrid at Heidelberg University.

References

[1] Ahmed, S. A., Giddens, D. P., *Journal of Biomechanics* **16**: 505–516 (1983).
[2] Zhang, Z., Kleinstreuer, C., and Kim, C. S., *Journal of Aerosol Science* **33(2)**: 1635–1652 (2002).
[3] Jayaraju, S.T., Brouns, M., Verbanck, S., and Lacor, C. , *Journal of Aerosol Science* **38**: 494-508 (2007).
[4] Corcoran, T. E., Chigier, N., *Journal of Biomechanical Engineering* **124**: 629 – 637 (2002).
[5] Cheng Y. S., *Aerosol Science and Technology* **37**: 659-671 (2003).
[6] Cheng, Y. S., Zhou, Y., and Chen, B. T., *Aerosol Science and Technology* **31**: 286–300 (1999).
[7] Kleinstreuer, C., Zhang, Z., *International Journal of Multiphase Flow* **29**: 271–89 (2003).
[8] Zhang, Z., Kleinstreuer, C., *Journal of Computational Physics* **198**: 178–210 (2004).
[9] Zhang, Z., Kleinstreuer, C., Donohue J. F., and Kim, C. S., *Journal of Aerosol Science* **36**: 211–33 (2005).
[10] Kleinstreuer, C., Zhang, Z., and Donohue, J. F., *Annual Review of Biomedical Engineering* **10**: 195–220 (2002).
[11] Stapleton, K.W., Guentsch, E., Hoskinson, M. K., and Finlay, W. H., *Journal of Aerosol Science* **31**: 739–49 (2000).
[12] Matida, E. A., Finlay, W. H., Lange, C. F., and Grgic, B., *Journal of Aerosol Science* **35**: 1–19 (2004).
[13] Brouns, M., Verbanck, S., and Lacor, C., *Journal of biomechanics* **40**: 165–72 (2007).
[14] Jin, H. H., Fan, J. R., Zeng, M. J., and Cen, K. F., J*ournal of Aerosol Science* **19**: 257–268 (2007).
[15] Ball, C. G., Uddin, M., and Pollard, A., *Computers and Fluids* **37**: 943–64 (2008).
[16] Ilie, M., Matida, E. A., and Finlay, W. H., *Aerosol Science and Technology* **42(1)**: 10 – 17 (2008).
[17] Kleinstreuer, C.; Zhang, Z., *Annual Review of Fluid Mechanics* 42: 301-334 (2009).
[18] Zhang, Z., Kleinstreuer, C., American Institute of Aeronautics and Astronautics Journal (AIAA J) **41**: 831–840 (2003).
[19] Jayaraju, S.T., Brouns, M., Lacor, C., Belkasse M, B., and S. Verbanck , S., *Journal of Aerosol Science* **39(10)**: 862-875 (2008).
[20] Luo, X. Y., Hinton, J. S., Liew, T. T., and Tan, K. K., *Medical Engineering and Physics* **26**: 403–413 (2004).
[21] Smargorinsky, J., *Monthly Weather Review* **91**: 99–164 (1963).
[22] Lippmann, M., Albert, R. E. *American Industrial Hygiene Association Journal* **30**: 257–275 (1969).
[23] Chan, T. L., Lippmann, M. *American Industrial Hygiene Association Journal* **41**: 399–409 (1980).
[24] Foord, N., Black, A., and Walsh, M. *Journal of Aerosol Science* **9**: 383–390 (1978).
[25] Stahlhofen, W., Gebhart, J., and Heyder, J. *American Industrial Hygiene Association Journal* **41**: 385–398 (1980).
[26] Stahlhofen, W., Gebhart, J., Heyder, J., and Scheuch, G. *Journal of Aerosol Science* **14**: 186–188 (1983).
[27] Emmett, P. C., Aitken, R. J., and Hannan, W. J. *Journal of Aerosol Science* 1**3**: 549–560 (1982).
[28] Bowes, S. M., Swift, D. L. *Aerosol Science and Technology* **11**: 157–167 (1989).
[29] Cui, X.-G., Gutheil, E., *Proc. International Conference on Multiphase Flows*, Tampa, FL, USA (2010).